

---

# Enter the Void - Planning to Seek Entropy When Reward is Scarce

---

**Ashish Sundar**

Department of Computer Science  
University of Exeter  
as1748@exeter.ac.uk

**Chunbo Luo**

Department of Computer Science  
University of Exeter  
c.luo@exeter.ac.uk

**Xiaoyang Wang**

Department of Computer Science  
University of Exeter  
x.wang7@exeter.ac.uk

## Abstract

Model-based reinforcement learning (MBRL) offers an intuitive way to increase the sample efficiency of model-free RL methods by simultaneously training a world model that learns to predict the future. MBRL methods have progressed by largely prioritising the actor; optimising the world model’s learning has been neglected meanwhile. Improving the world model’s fidelity and reducing its time to convergence can yield significant downstream benefits, one of which is improving the ensuing performance of any actor it may train. We propose a novel approach that anticipates and actively seeks out high-entropy states using the world model’s short-horizon latent predictions, offering a principled alternative to traditional curiosity-driven methods that chase once-novel states well after they were stumbled into. While many model predictive control (MPC) based methods offer similar alternatives, they typically lack commitment, synthesising multi step plans after every step. To mitigate this, we present a hierarchical planner that dynamically decides when to replan, planning horizon length, and the weighting between reward and entropy. While our method can theoretically be applied to any model that trains its own actors with solely model generated data, we have applied it to just Dreamer as a proof of concept. Our method finishes Miniworld’s procedurally generated mazes 50% faster than base Dreamer at convergence and the policy trained in imagination converges in only 60% of the environment steps that base Dreamer’s policy needs.

## 1 Introduction

In recent years, reinforcement learning (RL) has achieved remarkable success across a variety of domains, from mastering Go [Silver et al., 2017a] and optimising climate control [Evans and Gao, 2016] to quadruped locomotion [Lee et al., 2020] and high speed drone racing [Kaufmann et al., 2023]. However, these successes often rely on dense reward signals and highly structured environments. In real-world applications such as autonomous navigation, scientific exploration, and disaster response, rewards are sparse, environments are partially observable, and they are stochastic. In these conditions, achieving efficient exploration and good sample efficiency remain unsolved.

While shaping sparse rewards is a common solution, it is often impractical; curiosity-driven exploration offers a promising alternative. Contemporary high-performing curiosity-driven RL approaches [Pathak et al., 2017, Sekar et al., 2020, Burda et al., 2018, Zhelo et al., 2018, Houthoofd et al., 2016,

Bellemare et al., 2016] largely quantify novelty retrospectively by rewarding agents for revisiting novel states that were chanced upon in previous episodes. This retrospective approach limits real-time adaptability and is ineffective in non-stationary environments, where past novelty estimates quickly become obsolete. Anticipatory methods which predict the novelty of future states before acting offer greater adaptability but are typically limited to ensemble-based uncertainty estimations that fail in stochastic settings.

A promising direction to address these issues is model-based reinforcement learning (MBRL), where models of the environment (world models [Ha and Schmidhuber, 2018]) are concurrently trained to predict future observations. These world models can also train policy networks by simulating a virtual environment in conjunction with the policy network’s actions. Beyond improving sample efficiency and ensuring the actors always have access to on-policy data, world models inherently capture environmental dynamics and can be leveraged to estimate both reward uncertainty and transition uncertainty. Padding out the reward with reward uncertainty densifies a sparse reward signal, while seeking out transition uncertainty as an additional reward boosts training speed and stability. While world models are often treated as tools for facilitating policy learning, we adopt the antithesis: policies serve as mechanisms to accelerate and optimise world model training. By prioritizing the model’s epistemic gain during exploration, we ensure that policies operate not just to maximize reward but to actively improve the model’s understanding of its environment. This reframing enables the world model to generalize more effectively and support the training of robust downstream actors.

Prior work has also attempted to leverage model-based exploration but these approaches suffer from key limitations. Look before you leap [Wang et al., 2018] encourages agents to seek low-entropy, high-reward states which is effective only after training has converged. During training, this behavior leads to avoidance of uncertain or novel states, stalling learning and ultimately causing policy degradation. MaxEnt-Dreamer [Svidchenko and Shpilman, 2021] instead biases exploration toward high-entropy rollouts, but lacks any mechanism for plan commitment. The agent replans at every step and frequently abandons promising trajectories, undermining long-term exploration and reducing computational efficiency. RAIF [Nguyen et al., 2024] introduces a more nuanced objective: to maximize posterior uncertainty while minimizing prior uncertainty. However, this forces the agent to evaluate potential gains retrospectively, resulting in its inability to react to novel states as they appear.

In this work, we propose to augment Dreamer [Hafner et al., 2020], a prominent and efficient world model, with a planner to anticipate and seek informative states that drive structured exploration. We also introduce a lightweight PPO based hierarchical planner that uses model rollouts to dynamically select between high-entropy and high-reward trajectories and dynamically decide when to replan. While our experiments focus on Dreamer, our method is model-agnostic and can be applied to any MBRL framework that trains policies entirely through imagined trajectories. Although we do not explicitly combine our approach with alternative models in this work, the mathematical formulation of our method places no restrictions that would prevent doing so. However, we note that an inherent limitation of our method is the reliance upon a world model that can predict many states ahead with relatively low error rates. Further, we also require that the actor be trained purely with world model generated states rather than through experience replay, as we will bias collection of experiences towards effective training of the world model, leading to a distributional shift in the data relative to the actor’s policy.

Our contributions are:

- Leveraging world models’ transition uncertainty to predicting short-horizon state entropy and densify sparse rewards, accelerating training in MBRL.
- Reformulating the Dreamer KL minimization into an adversarial minmax objective to maximise information gain, enabling intelligent entropy driven exploration to directly optimise world model learning.
- Introducing a reactive hierarchical planner that dynamically selects between optimising entropy and reward while retaining the flexibility to discard the current plan and replan a new trajectory.

The rest of the paper is structured as follows. In Section 2, we review related work in intrinsic motivation, planning, and hierarchical RL. In Section 3, we provide background on Dreamer and

its training formulation. Section 4 introduces our entropy-seeking planner and reactive hierarchical policy. Section 5 details our experimental setup, evaluates performance on a procedurally generated 3D maze environment. Section 6 concludes this work and outlines limitations and subsequent directions for future work.

## 2 Related Work

### 2.1 Intrinsic Reward

Existing approaches to intrinsic reward can be separated into retrospective methods and anticipatory methods. Retrospective methods evaluate experiences after they have occurred and assign intrinsic reward based on metrics like prediction error [Pathak et al., 2017], state novelty [Burda et al., 2018], episodic novelty [Badia et al., 2020], or representation surprise [Raileanu and Rocktäschel, 2020]. These methods encourage agents to revisit novel states that were randomly discovered in past trajectories, and are typically implemented using model-free algorithms such as PPO, IMPALA, and A3C.

A known challenge for retrospective curiosity is the white noise problem [Burda et al., 2018], where agents are drawn to aleatoric uncertainty, stochastic but uninformative features, that yield consistently high prediction error. Since these rewards do not diminish with repeated exposure, agents may "farm" them, especially in sparse-reward settings. Another issue, detachment [Ecoffet et al., 2019], occurs when agents fail to return to previously discovered novel states as only the state is rewarded rather than the entire process utilised to get to that state.

Anticipatory methods instead attempt to steer agents toward potentially novel states before they have been visited by utilising short horizon predictions of epistemic uncertainty [Shyam et al., 2019, Sekar et al., 2020, Chua et al., 2018]. When combined with reward conditioning, they can better avoid aleatoric traps. However, these methods often require multi-step planning with dedicated predictive models, introducing significant architectural complexity and additional compute requirements. Overall, retrospective approaches are more popular due to their simplicity, lower implementation cost, and compatibility with standard model-free reinforcement learning algorithms—despite their known limitations.

### 2.2 Planning

While most RL agents act greedily without foresight, some of the most successful decision making AI systems explicitly model future outcomes. For example, Monte Carlo Tree Search (MCTS) [Coulom, 2006] played a key role in AlphaGo [Silver et al., 2016] and AlphaZero [Silver et al., 2017b], but MCTS relies on full observability and discrete action spaces, limiting its applicability to real-world stochastic settings.

Path integral control offers an alternative framework for planning under uncertainty by sampling and reweighting trajectories [Gómez et al., 2014, Williams et al., 2015], but classical implementations are computationally expensive. Neural network dynamics models alleviate this cost at the expense of precision and model calibration. TD-MPC (Temporal Difference - Model Predictive Control) and TD-MPC2 [Hansen et al., 2022, 2023] apply Model Predictive Path Integral (MPPI) style planning with Temporal Difference (TD) learning based policy optimization. However, their planners drift the actions away from the policy network, leading to distributional shift in the data and ensuing value overestimation.

### 2.3 Hierarchical Policies

Hierarchical reinforcement learning (HRL) provides a structured approach for addressing long-horizon credit assignment and decision-making by decomposing behavior into high-level and low-level control operating at different temporal scales. The low-level policy selects stepwise actions, while the high-level policy determines abstract actions or goals over extended horizons. A prominent approach in this field is Option-Critic (OC) [Bacon et al., 2017], where low-level actions are composed into options and executed. The critic is overloaded to determine when the actions executed as part of an option begin to return rewards lower than the baseline, at which point the option is terminated. HiPPO [Li et al., 2019] introduces a simpler alternative by running PPO at two predefined temporal

resolutions. However, this comes at the cost of flexibility, as it imposes fixed planning intervals and prohibits dynamic replanning or early termination.

### 3 Preliminaries

Dreamer [Hafner et al., 2019, 2020, 2023] learns a compact latent dynamics model and performs policy optimization entirely in latent space. At its core, Dreamer relies on a *Recurrent State Space Model* (RSSM) that factorizes the environment into deterministic recurrent states and stochastic latent representations. The RSSM is described by a series of formulations:

$$\begin{aligned} \text{Recurrent model: } h_t &= f_\phi(h_{t-1}, z_{t-1}, a_{t-1}) \\ \text{Transition predictor (prior): } \hat{z}_t &\sim p_\phi(\hat{z}_t | h_t) \\ \text{Representation model (posterior): } z_t &\sim q_\phi(z_t | h_t, x_t) \\ \text{Predictors (Image, Reward, Discount): } \hat{x}_t, \hat{r}_t, \hat{\gamma}_t &\sim p_\phi(\cdot | h_t, z_t) \end{aligned}$$

Here,  $x_t$  is the observation at time  $t$ , and  $h_t$  is the deterministic recurrent state. In the original Dreamer formulation, the autoencoder loss (an auxiliary loss) is given by a logarithmic loss that is applied through the image predictor as it reconstructs the image. In our implementation, we change the loss function to a combination of mean squared error (MSE) and an environment-specific reconstruction loss to accelerate convergence and improve early-stage feature alignment. This modification accelerates convergence and improves early-stage feature alignment by encouraging more stable and informative representations, facilitating effective downstream training from the latent space. Further details are provided in Appendix A.

The RSSM models the sequence of latent states  $z_t$  through a combination of different components, as detailed below. At each step, Dreamer generates a prior latent state  $\hat{z}_t$  from the deterministic recurrent state  $h_t$  via  $p(\hat{z}_t | h_t)$ , and updates it into a posterior  $q(z_t | h_t, x_t)$  once the new observation  $x_t$  has been received. The KL divergence between the prior and posterior is minimized to train the model:

$$\mathcal{L}_{\text{KL}} = \text{KL}[q(z_t | h_t, x_t) \| p(\hat{z}_t | h_t)] \quad (1)$$

Dreamer’s policy network is trained using imagined trajectories generated by the world model — specifically the prior predictor. Training batches are constructed by sampling random latent states from the replay buffer and rolling them out using the current policy and the prior predictor. This ensures that policy training remains effectively on-policy, regardless of the distribution of the sampled states. Aside from stabilizing techniques such as Exponential Moving Average (EMA), policy optimization in Dreamer largely relies on standard policy gradient methods. For completeness, the policy loss is provided below.

$$\text{Actor: } a_t \sim \pi_\theta(a_t | \hat{z}_t) \quad \text{Critic: } v_\psi(R_t | \hat{z}_t) \quad (2)$$

The loss of the critic is given as:

$$\mathcal{L}(\psi) = - \sum_{t=1}^T \ln p_\psi(R_t^\lambda | z_t) \quad (3)$$

where  $R_t^\lambda$  is the bootstrapped return. The loss of the actor is given as:

$$\mathcal{L}(\theta) \sim - \sum_{t=1}^T \left( \frac{R_t^\lambda - v_\psi(z_t)}{S} \right) \log \pi_\theta(a_t | z_t) + \eta \mathcal{H}(\pi_\theta(\cdot | z_t)) \quad (4)$$

where  $S$  is:

$$S \sim (\max(R_t^\lambda) - \min(R_t^\lambda))$$

While it is clear that the policy network’s training schema has been optimised, the buffer that the world model trains from is populated by a naive  $\epsilon$ -greedy actor. We show in this work that filling the buffer with high entropy transitions can lead to greater training efficiency and optimised exploration.

## 4 Method

### 4.1 Entropy

The latent states in Dreamer’s world model are modelled as stochastic latent variables drawn from a Gaussian distribution:

$$\hat{z}_t \sim \mathcal{N}(\mu_t, \Sigma_t) \quad (5)$$

We assume a diagonal Gaussian for tractability, so the covariance matrix  $\Sigma_t$  reduces to a vector of variances  $\sigma_t^2$ . We use  $\sigma_{p,i}$  to refer to the standard deviation along dimension  $i$  of the prior.

Training the model involves minimizing a KL divergence loss between the prior and posterior distributions (Equation (1)); the same KL divergence loss can also be interpreted as the model’s information gain (IG) about the environment at timestep  $t$  [Quinlan, 1986]

$$\text{IG} = \frac{1}{2} \left( k \frac{\sigma_q^2}{\sigma_p^2} + \frac{\|\mu_p - \mu_q\|^2}{\sigma_p^2} - k + k \log \left( \frac{\sigma_p^2}{\sigma_q^2} \right) \right) \quad (6)$$

When the model has trained long enough to become reasonably calibrated, the model should set  $\sigma_p$  and  $\mu_p$  such that any rise in  $\mu_p - \mu_q$  should be counterbalanced by a proportional increase in  $\sigma_p$ . Conversely,  $\mu_p - \mu_q \ll 1$  where  $\sigma_p$  is low.

Over time, the model naturally encourages  $\sigma_p$  to approach  $\sigma_q$  from above but not fall below  $\sigma_q$ . This behavior emerges because the magnitude of the gradient of information gain (or KL divergence loss) with respect to  $\sigma_p$ ,  $\left| \frac{d \text{IG}}{d \sigma_p} \right|$ , is greater when  $\sigma_p < \sigma_q$  than when  $\sigma_p \geq \sigma_q$ . As a result, the model is more strongly driven to increase  $\sigma_p$  when it overestimates certainty, leading to a self-correcting mechanism that helps maintain calibrated predictions and guards against overconfidence.

As a consequence, the most reliable way to increase information gain is by increasing  $\sigma_p$ , or where the model admits uncertainty. These are the places where learning is most likely to happen.

The entropy of the state’s distribution therefore can be taken as an estimate for the model’s uncertainty, as:

$$H(\sigma_p) = \frac{k}{2} \log(2\pi e) + \sum_{i=1}^k \log(\sigma_{p,i}) \quad (7)$$

where  $k$  is the dimensionality of the state. Thus, the objective becomes to maximise prior entropy:

$$\mathcal{J} = \max H(\sigma_p) \quad (8)$$

There are two primary failure modes for entropy-based exploration. The first arises in environments with high aleatoric uncertainty, where a state has multiple plausible successors due to stochasticity inherent to the environment. In these cases, even a well-understood state  $s_t$  may produce a high-entropy predictive distribution despite all potential outcomes being familiar. Suppose the environment’s true transition function satisfies:

$$p(s_{t+1} \mid s_t, a_t) > 0 \quad \text{for multiple distinct } s_{t+1}$$

The support of the distribution is therefore given by:

$$\text{Support}\left(p(s_{t+1} \mid s_t, a_t)\right) = \left\{ s_{t+1}^{(1)}, s_{t+1}^{(2)}, \dots, s_{t+1}^{(n)} \right\}$$

An ideal model would represent each successor with a low-variance Gaussian, forming a weighted mixture over plausible outcomes:

$$p^*(s_{t+1} \mid s_t, a_t) = \sum_{i=1}^n w_i \cdot \mathcal{N}(s_{t+1} \mid \mu_i, \sigma_i^2) \quad (9)$$

Here, each  $w_i$  represents the likelihood of observing the  $i$ -th successor state, satisfying  $\sum_{i=1}^n w_i = 1$ .

However, due to its unimodal predictive structure, the prior predictor must approximate a multi-modal distribution — comprised of several low-variance components — using a single Gaussian with inflated variance:

$$\hat{p}(s_{t+1} \mid s_t, a_t, h_{0:t}) \sim \mathcal{N}(\mu, \sigma^2), \quad \text{where } \sigma^2 > \sigma_i^2 \text{ for all } i$$

Here  $h_{0:t}$  denotes the history of recurrent hidden states up to time  $t$ .

In this case, elevated entropy arises from aleatoric uncertainty rather than epistemic uncertainty. To avoid over-exploration in these regions, we condition planning not solely on entropy but jointly on both entropy and predicted reward. The relative weighting of these objectives is state- and context-dependent, varying across the episode. To balance this trade-off effectively, we propose a hierarchical meta-policy that dynamically modulates the emphasis on reward maximization versus entropy during trajectory planning, as the optimal weighting may change through an episode.

The second failure mode arises in environments with latent transitions that require specific, rarely executed actions. In such cases, the ideal transition distribution remains:

$$p^*(s_{t+1} \mid s_t, a_t) = \sum_{i=1}^n w_i \cdot \mathcal{N}(s_{t+1} \mid \mu_i, \sigma_i^2) \quad (10)$$

Here, each mode corresponds to a distinct possible outcome, with weights  $w_i$  representing their respective likelihoods. The weight associated with the common transitions, denoted  $w_C$ , satisfies  $w_C \gg w_\varphi$ , where  $w_\varphi$  is the total weight of the rare transitions. If the agent has only encountered the high-probability transitions, the learned model will be ignorant of the rare outcomes and estimate:

$$\hat{p}(s_{t+1} \mid s_t, h_{0:t}) \sim \mathcal{N}(\mu, \sigma^2), \quad \text{where } \sigma^2 \ll 1$$

In these cases, a state’s uncertainty may be chronically underestimated and subsequently under-explored. This form of hidden epistemic uncertainty cannot be resolved by naïvely increasing entropy-seeking behavior globally or by enabling random exploration at all states. To mitigate such a problem, external semantic hints are required. While this is outside the scope of the present method, we hypothesize that using large language models (LLMs) to aid the SSM could enable the world model to incorporate such information through question-answering or tool use.

## 4.2 Reactive hierarchical planner

Building on Dreamer’s ability to roll out imagined trajectories, we introduce a planning mechanism that prioritizes high-entropy, high-reward trajectories to accelerate learning. At each interaction step, the agent rolls out  $N$  candidate trajectories (256 in our work) using the underlying greedy policy. Each trajectory is scored based on the entropy  $E_t$  of predicted states and the expected reward  $R_t$ . We define a combined objective, termed *endorphin*,  $D$ , as:

$$D = \frac{1}{H} \sum_t^{H+t-1} w_e E_t + (1 - w_e) R_t \quad (11)$$

where  $w_e \in [0, 1]$  controls the trade-off between exploration and exploitation over a planning horizon  $H$ .

The trajectory with the highest endorphin is selected. To decide whether to enact a plan, we introduce a stochastic hierarchical controller. A meta-policy outputs a discrete planning probability  $p_t \in \{0.00, 0.25, 0.50, 0.75, 1.00\}$ , and planning (or replanning) occurs if a uniformly sampled  $u_t \sim \mathcal{U}(0, 1)$  satisfies  $u_t < p_t$ . This stochastic mechanism introduces controlled noise into the planning process, similar to noising actions. Should the model choose the binary values of 1 or 0, planning becomes deterministic, allowing the meta policy to bypass the planning noise. The intermediate probabilities are discretized to balance expressive control with practical optimization. Introducing too many discrete decisions into an RL policy — particularly at the meta level — can degrade sample efficiency and destabilize training. Note that we do not include a cancel action as commonly done [Bacon et al., 2017], but instead the planner can choose to replace the current plan with a new one.

We find in practice that the planner tends to excessively replan, a finding echoed across the hierarchical RL literature [Klissarov et al., 2017] [Chunduru and Precup, 2022] [Johnson and Weitzenfeld, 2025], so we change the enaction expression from  $u_t < p_t$  to  $u_t < p_t^2$  to discourage excessive replanning.

The hierarchical controller comprises two meta-policies:

- Meta 1 outputs the planning horizon  $H$  and entropy-reward weighting  $w_e$ .
- Meta 2 outputs the planning probability  $p_t$ .

Importantly, planning decisions are re-evaluated at every environment step, allowing for flexible replanning without commitment if needed. Pseudocode for our planning algorithm is given in Appendix B.

To enable effective training of the meta-policy that governs planning frequency, it is essential that the agent is exposed to a sufficient diversity of planning behaviours early in learning. In particular, if the planning probability distribution collapses prematurely toward the extremes (i.e., always plan or never plan), the agent receives an impoverished set of trajectory candidates, preventing the meta-policy from learning when planning is actually beneficial. To mitigate this, we initialize the planning probability network using He initialization [He et al., 2015], followed by reordering the biases such that intermediate planning probabilities are more likely when compared to the more extreme values.

## 5 Experiments

We evaluate our approach in a procedurally generated 3D environment designed to emulate the partial observability and sparse rewards characteristic of real-world scenarios. The experiments aim to assess whether anticipatory planning and entropy-driven behavior improve exploration efficiency and downstream task performance.

### 5.1 Maze Explorer

We use a 3D maze environment adapted from MiniWorld [Chevalier-Boisvert et al., 2023], where each episode presents a new random layout. The agent receives RGB image observations and performs continuous actions to locate three goal boxes. We introduce a *porosity* parameter that controls wall density to vary exploration difficulty. Observations are augmented with a binary spatial map that encodes visited regions and current orientation, providing a simple episodic memory. The reward function combines exploration, proximity, and goal rewards to encourage both coverage and task success. Full environment details are in Appendix C.

### 5.2 Evaluation Methodology

Each agent is trained for 350,000 steps, a budget sufficient for Dreamer to converge. Owing to the procedural nature of the environment and the use of online learning, we evaluate generalization through training performance across diverse instantiations rather than a fixed test set.

We compare our method against:

- **Dreamer:** A strong model-based baseline.
- **PPO:** A widely used model-free method, given 256 extra on-policy episodes for fair comparison.

Model-free agents like PPO are known to struggle in MiniWorld’s mazes due to their limited memory and planning capabilities [Zha et al., 2021]. Full PPO implementation details are provided in Appendix D.

We report:

**Episode Length:** Steps required to complete the task (4096 if incomplete).

**KL Divergence:** KL between posterior and prior at the end of each episode, reflecting information gain.

**Prior Entropy:** Average entropy of the prior over sampled latent states, indicating predictive uncertainty.

All curves use a rolling average and standard deviation (window = 10% of data points).

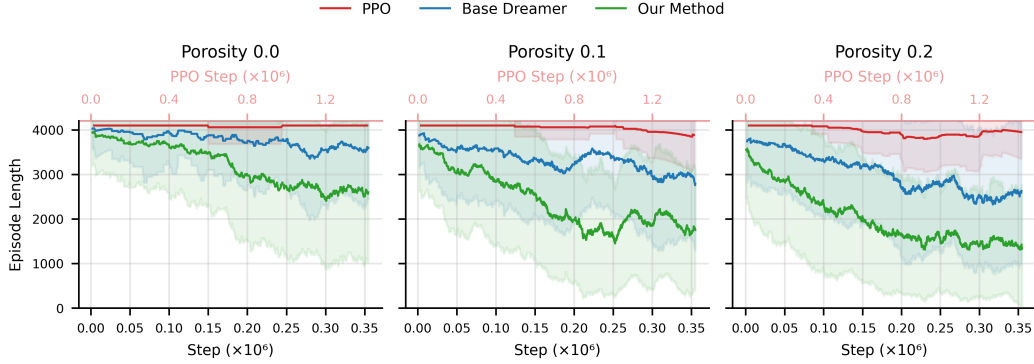


Figure 1: Episode lengths across different porosity levels. Lower porosity increases maze difficulty.

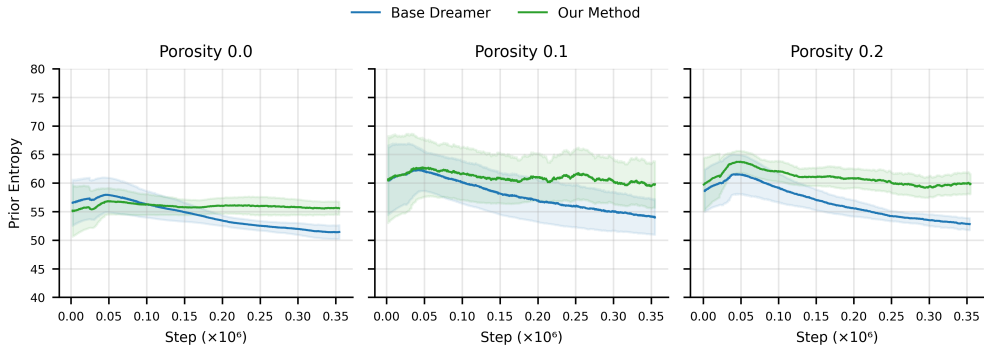


Figure 2: Prior entropies through different porosities, reflecting the model’s estimated uncertainty.

### 5.3 Experiments - Task Difficulty

Varying the porosity parameter controls maze difficulty. Visual examples of mazes at different porosity levels are provided in Appendix F. Figure 1 shows that our method maintains low episode lengths even in denser mazes, outperforming both Dreamer and PPO. PPO fails across all settings, likely due to its lack of memory and long-horizon reasoning. Dreamer’s performance degrades under low porosity, where rewards are harder to reach, while our method shows robust and consistent performance. Our method also exhibits lower variance, suggesting more consistent behavior across seeds.

Under the most difficult condition (porosity = 0), where only a single path exists between the agent and three goals, both our method and Dreamer perform worse. However, our approach still outperforms Dreamer, achieving 20% shorter episode lengths on average, albeit with higher variance due to the increased exploration burden.

Figure 2 shows that our method maintains approximately 10% higher prior entropy across training, indicating greater predictive uncertainty of the world model and a broader exploration strategy.

Figure 3 shows KL divergence values between the prior and posterior. Higher KL indicates that the world model is encountering states it cannot yet predict, which can reflect either model failure or valuable learning. Given that our method leads to better downstream performance, we interpret this as a sign of active, informative learning. KL divergence here functions as a min-max information gain signal: the agent seeks states that challenge the model, thereby improving imagination-based training while increasing KL divergence.

### 5.4 Ablation Study

To isolate the contributions of individual components, we compare:



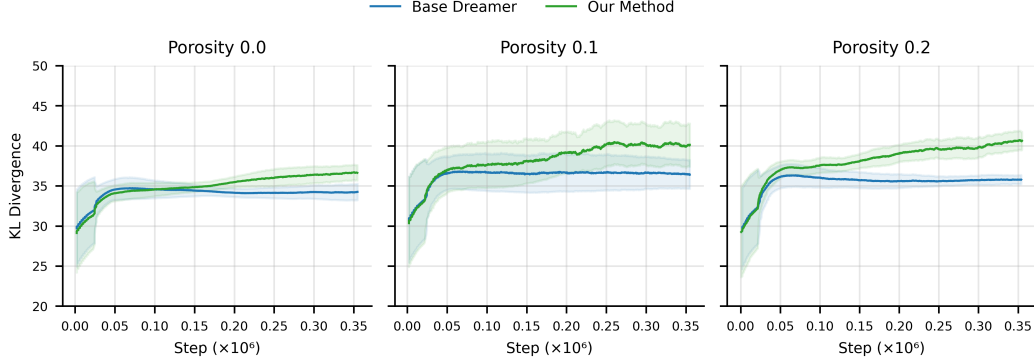
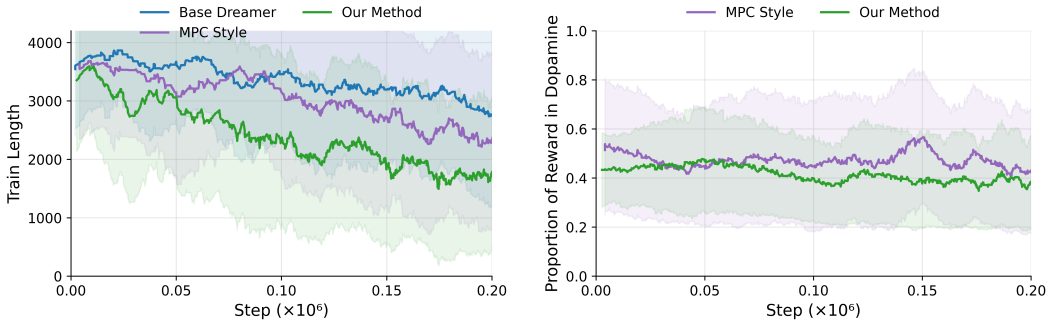


Figure 3: KL divergence across porosity levels. Higher porosity results in a more marked difference between our method and base Dreamer.



(a) Episode lengths during training for different ablations. The full planner outperforms both the base Dreamer and MPC-style variants, highlighting the benefit of plan commitment. (b) Ratio of entropy to reward in  $D$ , as set by meta 1. A high value of 1 here refers to all reward and no entropy and a low value of 0 refers to all entropy and no reward. The value balances reward and entropy rather than collapsing to either extreme.

Figure 4: Ablation study results. (a) Training performance under different planning variants. (b) Evolution of entropy-to-reward ratio during training.

**Base Dreamer:** The standard agent without planning.

**MPC Style:** To evaluate the value of our underlying planner, we modify the Meta 2 to replan at every step, mimicking MPC behaviour. Meta 1 remains trainable and flexible.

**Full Planner:** Our full method where we do not restrict the Meta 2.

We run all variants for 200,000 steps, which is sufficient for each to reach approximately 90% of its final performance. This threshold was chosen to reduce training time while still capturing meaningful differences in learning dynamics as performance gains beyond this point typically occur much more slowly.

This demonstrates the value of both the meta-policies and the planner, particularly the ability to commit to plans over extended horizons. Figure 4b further shows that the meta-policies do not exclusively prioritize reward or entropy. Instead, they maintain a dynamic balance, suggesting that both signals contribute meaningfully to effective planning, as reflected in PPO’s policy gradients over a 15-step horizon. Additional outputs from the meta-policies are provided in Appendix G.

## 6 Discussion

We present a robust method with fast convergence and a strong theoretical foundation to drive structured exploration in MBRL, suggesting it can generalize across domains and model architectures. While our experiments focus on a single environment and a single model, both represent challenging

benchmarks — the environment requires sophisticated exploration, and Dreamer is a state-of-the-art model. Future directions include enhancing the meta-policies with explicit mechanisms for long-term credit assignment. Improving this component to support temporally extended reasoning, while preserving its reactivity, could further enhance the adaptability and performance of the overall system. Extending this approach to more expressive world models, such as Transformer State Space Models (TSSMs), and to more diverse domains is another promising direction for future work.

## References

- David Silver, Julian Schrittwieser, Karen Simonyan, Ioannis Antonoglou, Aja Huang, Arthur Guez, Thomas Hubert, Lucas Baker, Matthew Lai, Adrian Bolton, et al. Mastering the game of go without human knowledge. *nature*, 550(7676):354–359, 2017a.
- Richard Evans and Jim Gao. Deepmind ai reduces google data centre cooling bill by 40%, July 2016. URL <https://deepmind.google/discover/blog/deepmind-ai-reduces-google-data-centre-cooling-bill-by-40/>. Accessed: 2025-05-12.
- Joonho Lee, Jemin Hwangbo, Lorenz Wellhausen, Vladlen Koltun, and Marco Hutter. Learning quadrupedal locomotion over challenging terrain. *Science robotics*, 5(47):eabc5986, 2020.
- Elia Kaufmann, Leonard Bauersfeld, Antonio Loquercio, Matthias Müller, Vladlen Koltun, and Davide Scaramuzza. Champion-level drone racing using deep reinforcement learning. *Nature*, 620(7976):982–987, 2023.
- Deepak Pathak, Pulkit Agrawal, Alexei A Efros, and Trevor Darrell. Curiosity-driven exploration by self-supervised prediction. In *International conference on machine learning*, pages 2778–2787. PMLR, 2017.
- Ramanan Sekar, Oleh Rybkin, Kostas Daniilidis, Pieter Abbeel, Danijar Hafner, and Deepak Pathak. Planning to explore via self-supervised world models. In *International conference on machine learning*, pages 8583–8592. PMLR, 2020.
- Yuri Burda, Harrison Edwards, Amos Storkey, and Oleg Klimov. Exploration by random network distillation. *arXiv preprint arXiv:1810.12894*, 2018.
- Oleksii Zhelo, Jingwei Zhang, Lei Tai, Ming Liu, and Wolfram Burgard. Curiosity-driven exploration for mapless navigation with deep reinforcement learning. *arXiv preprint arXiv:1804.00456*, 2018.
- Rein Houthooft, Xi Chen, Yan Duan, John Schulman, Filip De Turck, and Pieter Abbeel. Vime: Variational information maximizing exploration. *Advances in neural information processing systems*, 29, 2016.
- Marc Bellemare, Sriram Srinivasan, Georg Ostrovski, Tom Schaul, David Saxton, and Remi Munos. Unifying count-based exploration and intrinsic motivation. *Advances in neural information processing systems*, 29, 2016.
- David Ha and Jürgen Schmidhuber. World models. *arXiv preprint arXiv:1803.10122*, 2018.
- Xin Wang, Wenhan Xiong, Hongmin Wang, and William Yang Wang. Look before you leap: Bridging model-free and model-based reinforcement learning for planned-ahead vision-and-language navigation. In *Proceedings of the European Conference on Computer Vision (ECCV)*, pages 37–53, 2018.
- Oleg Svidchenko and Aleksei Shpilman. Maximum entropy model-based reinforcement learning. *arXiv preprint arXiv:2112.01195*, 2021.
- Viet Dung Nguyen, Zhizhuo Yang, Christopher L Buckley, and Alexander Ororbia. R-aif: Solving sparse-reward robotic tasks from pixels with active inference and world models. *arXiv preprint arXiv:2409.14216*, 2024.
- Danijar Hafner, Timothy Lillicrap, Mohammad Norouzi, and Jimmy Ba. Mastering atari with discrete world models. *arXiv preprint arXiv:2010.02193*, 2020.
- Adrià Puigdomènech Badia, Pablo Sprechmann, Alex Vitvitskyi, Daniel Guo, Bilal Piot, Steven Kapturowski, Olivier Tieleman, Martín Arjovsky, Alexander Pritzel, Andrew Bolt, et al. Never give up: Learning directed exploration strategies. *arXiv preprint arXiv:2002.06038*, 2020.
- Roberta Raileanu and Tim Rocktäschel. Ride: Rewarding impact-driven exploration for procedurally-generated environments. *arXiv preprint arXiv:2002.12292*, 2020.
- Adrien Ecoffet, Joost Huizinga, Joel Lehman, Kenneth O Stanley, and Jeff Clune. Go-explore: a new approach for hard-exploration problems. *arXiv preprint arXiv:1901.10995*, 2019.
- Pranav Shyam, Wojciech Jaśkowski, and Faustino Gomez. Model-based active exploration. In *International conference on machine learning*, pages 5779–5788. PMLR, 2019.
- Kurtland Chua, Roberto Calandra, Rowan McAllister, and Sergey Levine. Deep reinforcement learning in a handful of trials using probabilistic dynamics models. *Advances in neural information processing systems*, 31, 2018.

- Rémi Coulom. Efficient selectivity and backup operators in monte-carlo tree search. In *International conference on computers and games*, pages 72–83. Springer, 2006.
- David Silver, Aja Huang, Chris J Maddison, Arthur Guez, Laurent Sifre, George Van Den Driessche, Julian Schrittwieser, Ioannis Antonoglou, Veda Panneershelvam, Marc Lanctot, et al. Mastering the game of go with deep neural networks and tree search. *nature*, 529(7587):484–489, 2016.
- David Silver, Thomas Hubert, Julian Schrittwieser, Ioannis Antonoglou, Matthew Lai, Arthur Guez, Marc Lanctot, Laurent Sifre, Dhharshan Kumaran, Thore Graepel, et al. Mastering chess and shogi by self-play with a general reinforcement learning algorithm. *arXiv preprint arXiv:1712.01815*, 2017b.
- Vicenç Gómez, Hilbert J Kappen, Jan Peters, and Gerhard Neumann. Policy search for path integral control. In *Machine Learning and Knowledge Discovery in Databases: European Conference, ECML PKDD 2014, Nancy, France, September 15-19, 2014. Proceedings, Part I 14*, pages 482–497. Springer, 2014.
- Grady Williams, Andrew Aldrich, and Evangelos Theodorou. Model predictive path integral control using covariance variable importance sampling. *arXiv preprint arXiv:1509.01149*, 2015.
- Nicklas Hansen, Xiaolong Wang, and Hao Su. Temporal difference learning for model predictive control. *arXiv preprint arXiv:2203.04955*, 2022.
- Nicklas Hansen, Hao Su, and Xiaolong Wang. Td-mpc2: Scalable, robust world models for continuous control. *arXiv preprint arXiv:2310.16828*, 2023.
- Pierre-Luc Bacon, Jean Harb, and Doina Precup. The option-critic architecture. In *Proceedings of the AAAI conference on artificial intelligence*, volume 31, 2017.
- Alexander C Li, Carlos Florensa, Ignasi Clavera, and Pieter Abbeel. Sub-policy adaptation for hierarchical reinforcement learning. *arXiv preprint arXiv:1906.05862*, 2019.
- Danijar Hafner, Timothy Lillicrap, Jimmy Ba, and Mohammad Norouzi. Dream to control: Learning behaviors by latent imagination. *arXiv preprint arXiv:1912.01603*, 2019.
- Danijar Hafner, Jurgis Pasukonis, Jimmy Ba, and Timothy Lillicrap. Mastering diverse domains through world models. *arXiv preprint arXiv:2301.04104*, 2023.
- J. Ross Quinlan. Induction of decision trees. *Machine learning*, 1:81–106, 1986.
- Martin Klissarov, Pierre-Luc Bacon, Jean Harb, and Doina Precup. Learnings options end-to-end for continuous action tasks. *arXiv preprint arXiv:1712.00004*, 2017.
- Raviteja Chunduru and Doina Precup. Attention option-critic. *arXiv preprint arXiv:2201.02628*, 2022.
- Brendon Johnson and Alfredo Weitzenfeld. Hierarchical reinforcement learning in multi-goal spatial navigation with autonomous mobile robots. *arXiv preprint arXiv:2504.18794*, 2025.
- Kaiming He, Xiangyu Zhang, Shaoqing Ren, and Jian Sun. Delving deep into rectifiers: Surpassing human-level performance on imagenet classification. In *Proceedings of the IEEE international conference on computer vision*, pages 1026–1034, 2015.
- Maxime Chevalier-Boisvert, Bolun Dai, Mark Towers, Rodrigo de Lazcano, Lucas Willems, Salem Lahlou, Suman Pal, Pablo Samuel Castro, and Jordan Terry. Minigrid & miniworld: Modular & customizable reinforcement learning environments for goal-oriented tasks. *CoRR*, abs/2306.13831, 2023.
- Daochen Zha, Wenye Ma, Lei Yuan, Xia Hu, and Ji Liu. Rank the episodes: A simple approach for exploration in procedurally-generated environments. *arXiv preprint arXiv:2101.08152*, 2021.

## A Task-Aware Reconstruction Loss, RSSM

Dreamer’s reconstruction objective is trained jointly with its reward and transition models. However, we find that the standard loss formulation often neglects sparse, task-relevant visual features early in training. In particular, elements such as single-colour goal boxes and proximity indicators are frequently underemphasized until shaped by downstream reward gradients. This delayed encoding limits sample efficiency and impedes the development of a semantically rich latent space.

To address this, we propose a task-aware reconstruction loss built upon four primary components, designed to upweight critical areas of the observation. Let  $\hat{y}$  denote the reconstructed observation and  $y$  the ground truth. The total loss is defined as:

$$\mathcal{L}_{\text{recon}} = \lambda_{\text{MSE}} \cdot \mathcal{L}_{\text{MSE}} + \lambda_{\text{MAE}} \cdot \mathcal{L}_{\text{MAE}} + \lambda_{\text{SSIM}} \cdot \mathcal{L}_{\text{SSIM}} \quad (12)$$

- The MSE loss captures low-frequency structure.

$$\mathcal{L}_{\text{MSE}} = \|\hat{y} - y\|_2^2 \quad (13)$$

- The MAE loss featuring spatial and semantic weighting promotes fidelity in key regions.

$$\mathcal{L}_{\text{MAE}} = \sum_i w_i \cdot |\hat{y}_i - y_i| \quad (14)$$

where  $w_i$  is a per-pixel weight based on semantic role. For instance:

- Goal box colors (red, green, blue):  $w = 16$
- Proximity bar region:  $w = 20$
- Agent position and heading on the map:  $w = 35$
- The SSIM loss encourages high-frequency perceptual fidelity.

$$\mathcal{L}_{\text{SSIM}} = 1 - \text{SSIM}(\hat{y}, y) \quad (15)$$

The weights used internally are  $\lambda_{\text{MSE}} = 0.5$ ,  $\lambda_{\text{MAE}} = 0.5$ , and  $\lambda_{\text{SSIM}} = 1.0$ . These terms are applied independently across the image and map channels of the observation, and their final sum forms the decoder’s contribution to the overall world model loss.

Qualitatively, we observe that adding these terms enables consistent reconstruction of task-relevant visual semantics even in early training. To ensure fairness in evaluation, we also extend the base Dreamer model with this modified reconstruction loss during ablation and baseline comparison experiments.

While we modify the encoder’s loss function to improve the latent encoding and the speed with which a latent space is converged upon, we do not modify the underlying Recurrent State-Space Model (RSSM) in any way for the purposes of this study.

Dreamer models the environment using an RSSM, utilising a Gated Recurrent Unit (GRU), a recurrent neural network, to capture temporal dynamics that preserves context. The RSSM operates in latent space which is produced by the encoder and refined by the decoder. The RSSM separates the state into a deterministic component  $h_t$ , which is the direct output of the GRU, and a stochastic component  $z_t$  which is produced by the prior model when given  $h_t$ . The decoder operates upon the posterior representation, which processes the encoded representation with the prior’s output.

At each timestep  $t$ , RSSM updates the belief over latent states using:

$$h_t = \text{GRU}(h_{t-1}, [z_{t-1}, a_{t-1}]) \quad (16)$$

$$z_t \sim p(z_t | h_t) \quad (\text{prior}) \quad (17)$$

$$z_t \sim q(z_t | h_t, e_t) \quad (\text{posterior}) \quad (18)$$

where  $e_t$  is the encoded observation and  $a_{t-1}$  is the previous action.

The posterior  $q$  is only used during training for reconstruction and KL divergence regularization. The prior  $p$  is used for imagination and planning. The concatenated latent state  $s_t = [h_t, z_t]$  is then passed to heads for reward prediction, continuation, entropy estimation, and reconstruction.

The use of a GRU for the deterministic hidden state  $h_t$  makes the RSSM both lightweight and computationally efficient. GRUs have lower inference time and fewer parameters than more complex sequence models such as transformers. While GRUs operate with linear computational complexity in the sequence length, transformers typically incur quadratic complexity due to their full self attention mechanism. This makes GRUs especially well suited for online model-based reinforcement learning, where efficiency and speed are critical.

By combining temporal recurrence with structured stochasticity, RSSM allows Dreamer to learn accurate and temporally coherent world models, while remaining computationally efficient.

## B Planning Algorithm

---

### Algorithm 1 Entropy Seeking Anticipatory Planning

---

- 1: **Input:** Observation  $o_t$
  - 2: Meta-policy 1 selects planning horizon  $H$  and entropy weight  $w_e$
  - 3: Meta-policy 2 computes discrete planning probability  $p_t \in \{0, 0.05, 0.25, 0.55, 1\}$  (via squaring sampled values from  $\{0, 0.25, 0.5, 0.75, 1.0\}$ )
  - 4: Sample  $u_t \sim \mathcal{U}(0, 1)$
  - 5: **if**  $u_t < p_t$  **then**
  - 6:   Greedy actor samples  $C$  candidate actions  $a_1, \dots, a_C$  from  $o_t$
  - 7:   **for**  $i = 1$  to  $C$  **do**
  - 8:     Roll out trajectory  $\tau_i$  of length  $H$  using world model and greedy actor
  - 9:     Compute  $D_i = \frac{1}{H} \sum_{t=1}^H w_e E_t^{(i)} + (1 - w_e) R_t^{(i)}$
  - 10:   Select trajectory  $\tau_{best} = \arg \max D_i$
  - 11:   Set plan to  $\tau_{best}$
  - 12: Continue interacting with environment; repeat planning check at next step
- 

## C Miniworld Environment and Reward Scheme

We extend the MiniWorld Maze environment [Chevalier-Boisvert et al., 2023] with several task relevant augmentations. The maze environment is a 3 dimensional procedurally generated maze of size 8x8 (using recursive backtracking) where the agent can take continuous actions along three dimensions - forward/back (step size attenuated if moving backwards to encourage progress), strafe left/right, turn left/right. Each observation consists of a forward-facing RGB image of size (64x64x3). Each episode ends when the time limit (4096) is reached, or the three goal boxes have been found. Each training run samples a new maze structure every episode to prevent memorization. No regions of the maze are sectioned off from the rest of the maze and all the goal states are reachable.

To promote structured exploration, we introduce a porosity parameter that controls wall density: with probability  $p$ , wall segments are randomly removed during generation. This provides a tunable complexity gradient for navigation tasks by creating variable maze connectivity.

An auxiliary binary 2D map of size (64x64x3) that records agent visitation over the course of an episode has been concatenated to the observation. This map records visited coordinates as 1s whereas unvisited coordinates are kept at 0. The position of the agent and the direction it is looking in is also visible on the map. This serves as episodic spatial memory that enables agents to reason about coverage and connect their actions to the current observation. This mirrors plausible real-world capabilities that can be enacted through GPS tracking or odometry.

The reward function consists of three components:

**Exploration Reward:** A positive reward is granted when the agent visits a previously unvisited cell in its binary exploration map. The reward magnitude is proportional to the number of newly visited cells within a square region around the agent, the size of which is controlled by the *blur* parameter, given by  $b$ . While this reward introduces non-Markovian dynamics by incorporating visitation history, the inclusion of a binary map in the observation allows memory-less model-free agents such as PPO to perform effectively in this environment.

$$\text{exploration reward} = \begin{cases} \frac{\Delta_t}{b^2} & \text{if } b > 1 \\ \Delta_t & \text{otherwise} \end{cases}$$

where  $\Delta_t$  = number of newly explored cells at time  $t$

**Proximity Reward:** A smoothly decaying signal is emitted by each goal object, with exponentially scaled rewards given when the agent is within an  $x$ -unit radius. This mimics real-world analogs such as bluetooth signals or radio signals for search and rescue, animal noises for ecological monitoring, or semantic hints for more advanced exploration. This reward takes the form of two bars in the center of the image - if the agent is near a goal box of a particular colour (red, green, or blue), the bars will turn that colour with intensity varying with distance.

$$\text{Proximity reward} = \begin{cases} 0 & \text{if } \Delta < 0 \text{ or } \Delta > 10 \\ (10 - \Delta)^2 \cdot p_{mul} & \text{otherwise} \end{cases}$$

where  $\Delta = \text{dist} - (r_{\text{agent}} + r_{\text{box}} + s)$  and  $p_{mul} = 0.03$

**Goal Reward:** The agent gets a reward for moving into a coloured box. It gets 50 per box and then 150 when it gets the third box.

Thus the overall reward is composed of these three elements summed onto the baseline of -10. The lower limit of reward gained in an episode is  $-T$  where  $T$  is the time limit, and the upper limit is 0.

## D PPO Experiment Details

We use Ray RLlib’s implementation of PPO as our model-free baseline. PPO is a strong general-purpose algorithm, but its performance tends to degrade in tasks with sparse rewards and partial observability, such as MiniWorld’s procedurally generated mazes [Zha et al., 2021]. As PPO is strictly on-policy, it cannot benefit from the same random rollout pretraining used in model-based methods like Dreamer. To ensure a fair comparison, we provide PPO with an additional 256 on-policy training episodes instead of initialising it with previously collected random walk data as we do with the model based methods.

PPO receives the same augmented observations as Dreamer, including the first-person RGB view and the auxiliary spatial map. We also enable frame stacking and maintain RGB color to support temporal and visual understanding during navigation.

### PPO-Specific Parameters

- PPO Steps: 1,398,576
- Rollout Fragment Length: 512
- Train Batch Size: 16,384
- SGD Minibatch Size: 2,048
- Number of SGD Iterations: 10
- Gradient Clipping: 0.5
- Learning Rate:  $3 \times 10^{-5}$
- Gamma (Discount): 0.995
- Clipping Parameter: 0.1
- Entropy Coefficient: 0.001
- Value Function Loss Coefficient: 1.0
- KL Target: 0.01

## E Experiment Configuration

This appendix details the configuration used in all experiments. Our setup is based on the Dreamer framework with extensions for hierarchical planning. We include hyperparameters for the model architecture, training schedule, environment, and planning modules to support full reproducibility.

To our surprise, MiniWorld appears to be significantly more CPU-bound than GPU-bound, likely due to its lightweight rendering and Python-based simulation. For example, 350,000 training steps took 16 hours on a system with an NVIDIA 5090 GPU and an Intel i9-14900K (24 cores, 6.0 GHz max), compared to 24 hours on an NVIDIA 4090 GPU paired with a 13th Gen i7-13700K (16 cores, 5.4 GHz max), and 36 hours on an NVIDIA 4070 Ti GPU with an AMD Ryzen 9 5900X (12 cores, 4.8 GHz max). These differences suggest that CPU core count and clock speed significantly influence throughput in MiniWorld environments, even when powerful GPUs are available.

### E.1 Environment

- **Environment Name:** MiniWorld-MazeCA-v0
- **Time Limit:** 4096 steps per episode
- **Action Repeat:** 1
- **Parallel Environments:** 1
- **Porosity:** Varied across experiments; see Appendix F for visualizations

## E.2 Model Architecture

- **Latent State:** 512-dimensional deterministic + 32-dimensional discrete stochastic
- **Recurrent Depth:** 2 (GRU)
- **Encoder (Visual / Map):** 5-layer MLPs with CNNs, `cnn_depth=64`, `kernel_size=4`
- **Decoder:** Decodes both image and map, uses `mae` and `symlog_mse` losses
- **Activation Function:** SiLU; normalization enabled
- **Gradient Heads:** decoder, reward, cont, entropy
- **Initial Distribution:** Learned

## E.3 Actor and Critic

- **Actor:** 2-layer MLP, normal distribution, entropy regularization  $3e-4$
- **Critic and Q-function:** 2-layer MLPs, `symlog_disc` distribution
- **Learning Rate:**  $3e-5$ , **Gradient Clipping:** 100.0

## E.4 Training Configuration

- **Precision:** 16-bit
- **Batch Size:** 16
- **Batch Length:** 64
- **Model Learning Rate:**  $1e-4$
- **Optimizer:** Adam, `eps=1e-8`
- **Dataset Size:** 1,048,576
- **Train Ratio:** 2
- **Train Steps per Update:** 1

## E.5 Planning Behavior (Hierarchical)

- **Planning Horizon:** 15 steps
- **Plan Choices:** 256
- **Meta-Policy Input Dimensions:**
  - Higher-level: 11272
  - Lower-level: 9734
- **Training Frequency:** Every 32 steps
- **Learning Rate:** 0.003
- **Entropy Regularization:** 0.1

## E.6 Replay Buffer and PPO-style Update

- **Buffer Size:** 32,768
- **Minimum Samples Before Training:** 128
- **Clipping  $\epsilon$ :** 0.2
- **Discount Factor  $\gamma$ :** 0.99
- **GAE  $\lambda$ :** 0.95

## E.7 Maze and Observation Configuration

- **Observation Size:**  $64 \times 64 \times 3$
- **Domain Randomization:** Disabled
- **Fluff Factor:** 2
- **Map Input:** Included (`include_maps=True`)



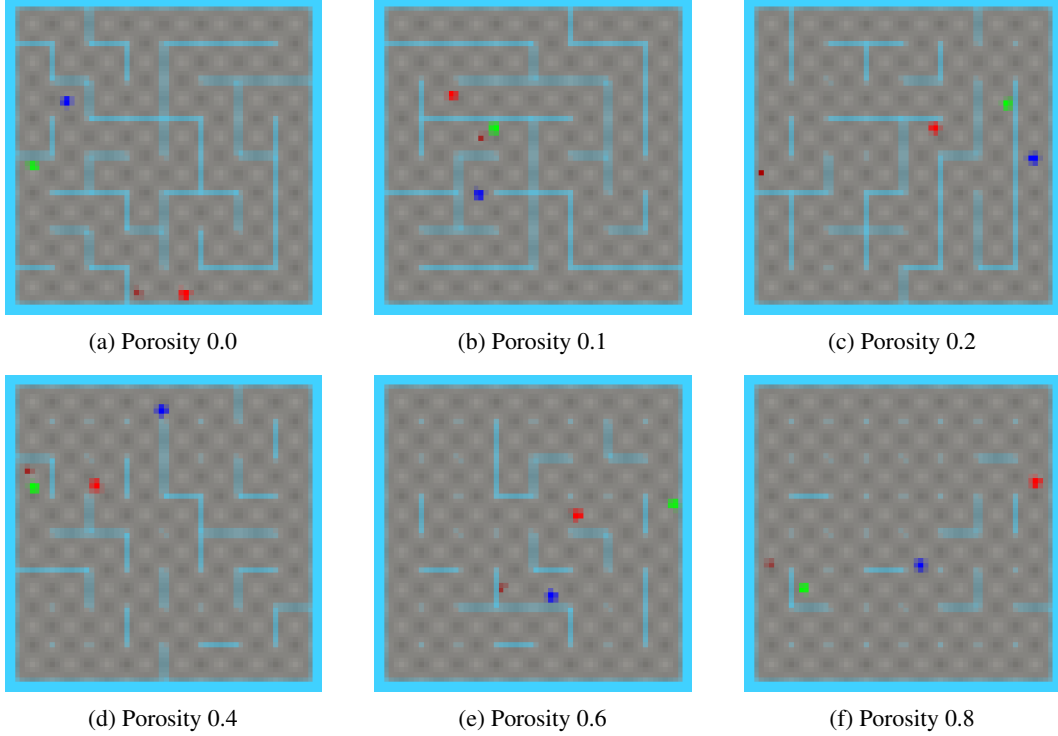


Figure 5: Top-down maze layouts at selected porosity levels. Higher porosity values remove more internal walls, increasing openness and reducing planning difficulty.

## F Maze Images

To visualize the effect of varying porosity on maze complexity, we provide top-down views of generated mazes at increasing porosity levels, see Fig. 5. As porosity increases, more internal walls are removed, resulting in more open environments. These top-down maps reflect the structural differences that influence planning difficulty.

To contextualize the agent’s perspective within these mazes, we also provide an example of the full map layout and a corresponding visual observation seen by the agent, as given in Figure 6.

## G Other Results

In this section, we present additional metrics and quantities tracked during our experiments. While these results are not central to the main text, they provide further insight into the model’s internal behavior and performance dynamics.

From the porosity comparison study, we highlight the internal planning parameters set by the meta-policy. Specifically:

- The endorphin ratio between reward and entropy is shown in Figure 7, with intra-episode standard deviation in Figure 8.
- The probability of replanning is shown in Figure 9, with its intra-episode standard deviation in Figure 10.
- The planning horizon is shown in Figure 11, with its intra-episode standard deviation in Figure 12.

Shaded intervals in all graphs represent variation across different random seeds, while intra-episode standard deviations are shown in dedicated plots.

We begin by examining how the meta-policy adjusts the balance between reward and entropy during planning. Figure 7 illustrates the endorphin ratio, a proxy for this trade-off, across different porosities and training steps. This ratio remains relatively stable overall, though minor variations emerge depending on environment difficulty and training stage. To understand how this behavior fluctuates within individual episodes, Figure 8 presents the intra-episode standard deviation of the endorphin ratio. These deviations tend to decrease as porosity increases, suggesting more consistent decision-making in easier environments.

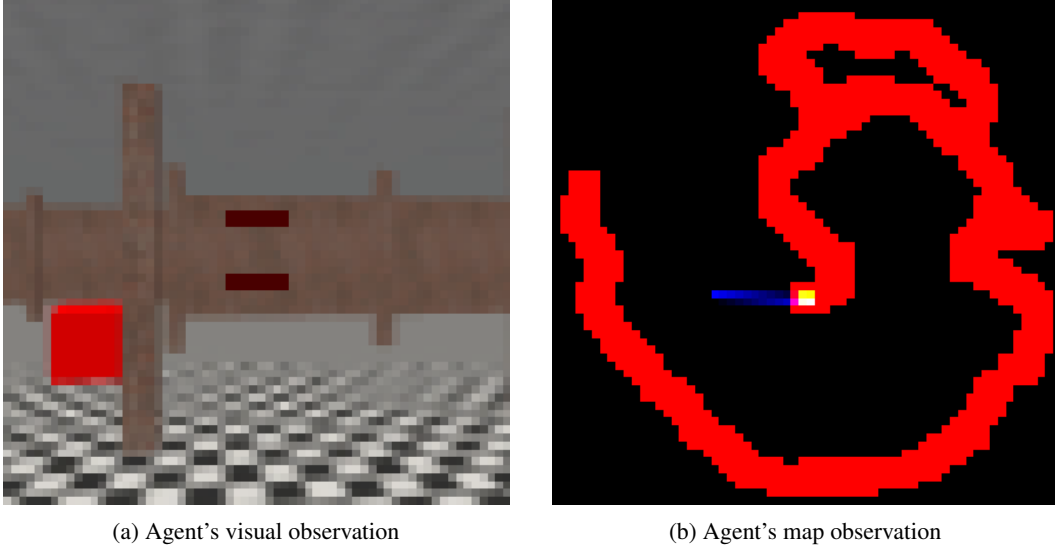


Figure 6: Image of what the agent perceives - the visual observation (left) and of the map observation (right).

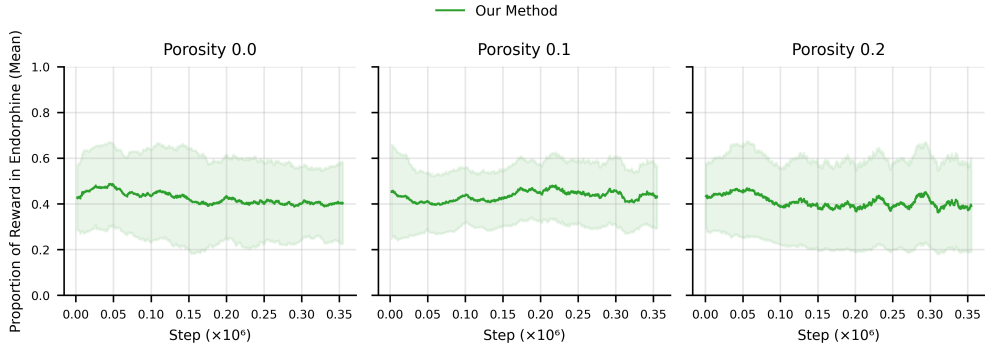


Figure 7: Endorphin ratios across different porosities. Although the ratios remain relatively stable across porosities and training time, slight variation is observed.

Next, we explore the replanning probability, which captures how often the agent updates its plan mid-episode. Figure 9 shows the average replanning probabilities over training for each porosity level. While the means are broadly similar, a clear reduction in variability across seeds is observed at higher porosities, reflecting more deterministic behavior under lower uncertainty. Figure 10 complements this by plotting the intra-episode standard deviation of the replanning probability. Here, we observe a steady decline over training, indicating growing confidence in the agent's planning under all conditions.

Finally, Figures 11 and 12 focus on the planning horizon, which represents how far ahead the meta-policy attempts to predict. As shown in Figure 11, planning horizons increase in more predictable (high-porosity) environments, whereas more challenging settings result in slower growth and greater inter-seed variance. The intra-episode standard deviations in Figure 12 remain relatively uniform across porosities but exhibit a slight downward trend, reflecting the stabilizing influence of meta-policy convergence during training.

Figure 13 presents the actor loss across different porosities, indicating that our method does not significantly affect the actor component itself, but instead the gains in performance are driven by directly optimising the world model. Interestingly, a divergence between the planned and unplanned variants becomes apparent toward the end of training in the 0.2 porosity setting. This may suggest that, as the world model converges and its predictive uncertainty decreases, the actor also stabilizes and its loss declines. Additionally, the standard deviation of the actor loss is notably lower for the planned agent in higher-porosity environments, which is likely a consequence of reduced epistemic uncertainty in the world model.

Figure 14 presents the length of a plan before replanning occurs. This measure is generally stable across porosities, but the variance across seeds is higher in more difficult (low porosity) settings. Interestingly, as

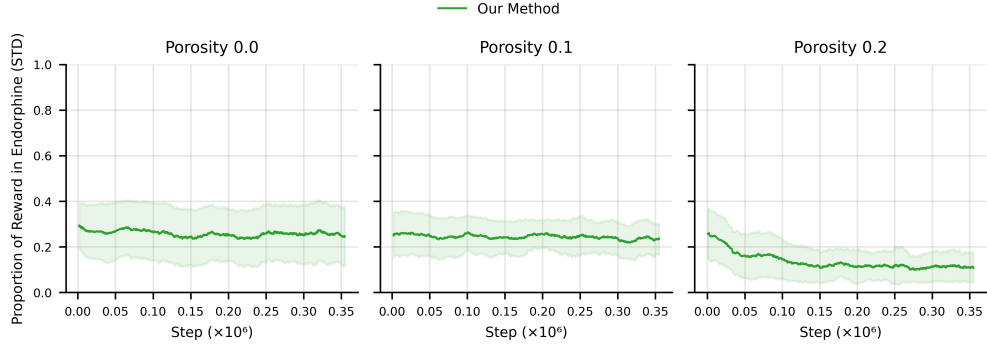


Figure 8: Intra-episode standard deviations of endorphin ratios. The deviation decreases as porosity increases, suggesting more stable planning under easier conditions.

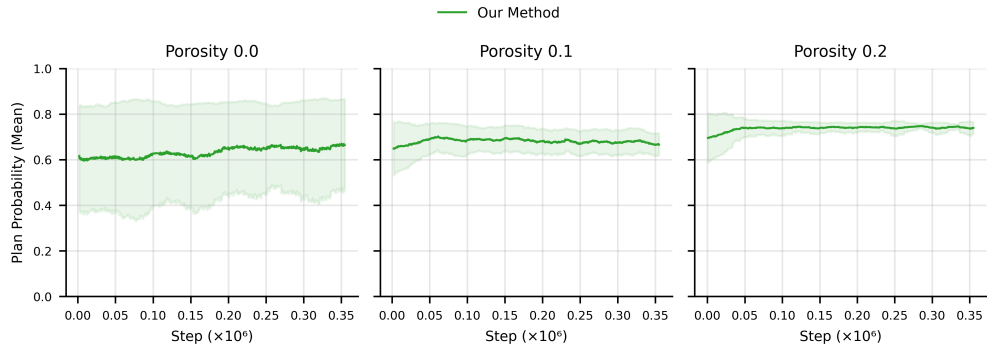


Figure 9: Replanning probabilities across porosities. While mean values remain comparable, variance across seeds diminishes faster at higher porosities.

shown in Figure 15, the intra-episode standard deviation remains low, suggesting that while different seeds may converge to distinct stable values, intra-run variability remains small. The variation between seeds in Figure 15 is higher in the hardest setting, as noted in previous plots. This could be because of the world model not reaching convergence as easily.

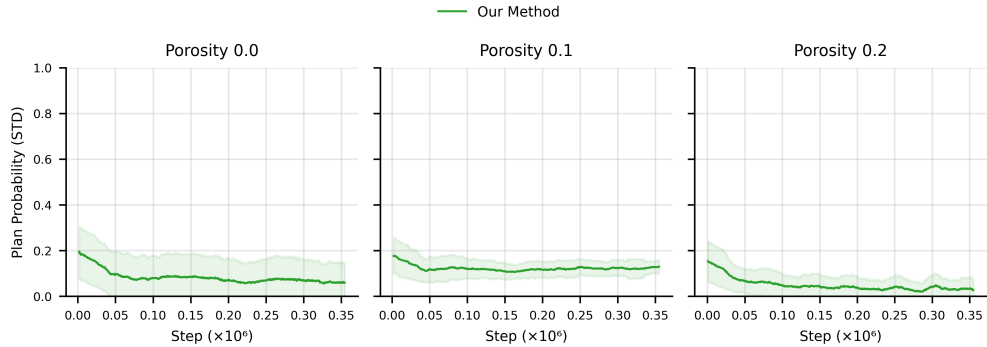


Figure 10: Intra-episode standard deviations of replanning probabilities. These deviations drop quickly as meta-policies converge.

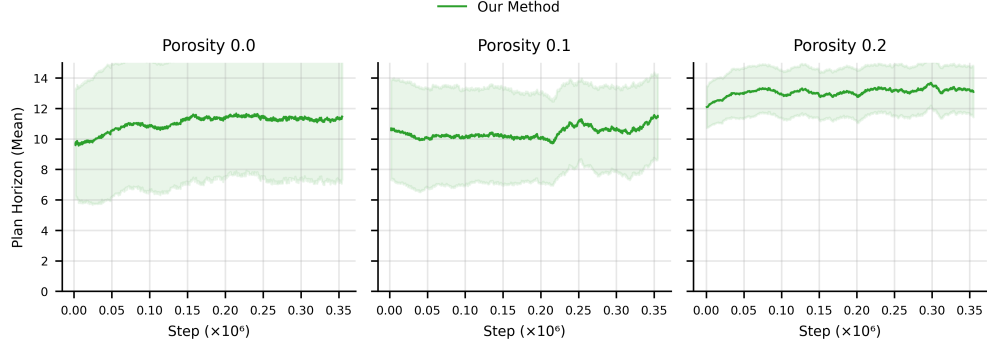


Figure 11: Planning horizons across porosities. Horizons increase as model fidelity improves, particularly for high-porosity environments. In low-porosity settings, horizons rise more gradually, and variance across seeds is higher.

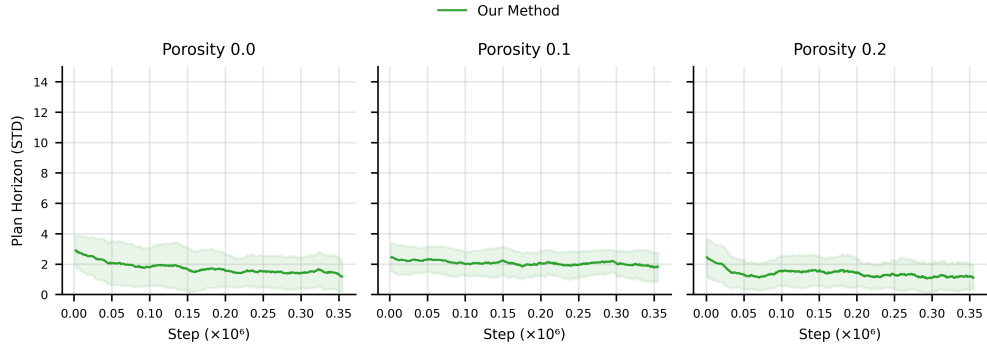


Figure 12: Intra-episode standard deviations of planning horizons. The deviations are relatively consistent across porosities, with a slight decline over training as the meta policy converges.

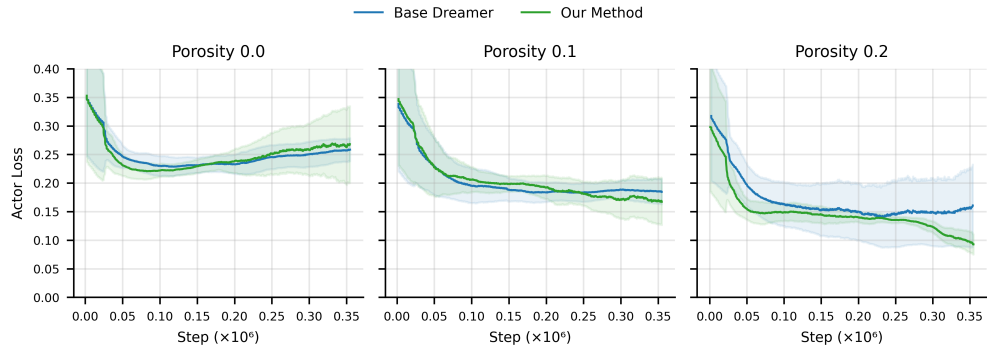


Figure 13: Actor loss across porosities. The actor remains stable across planning variants, with some divergence occurring later in training for 0.2 porosity.

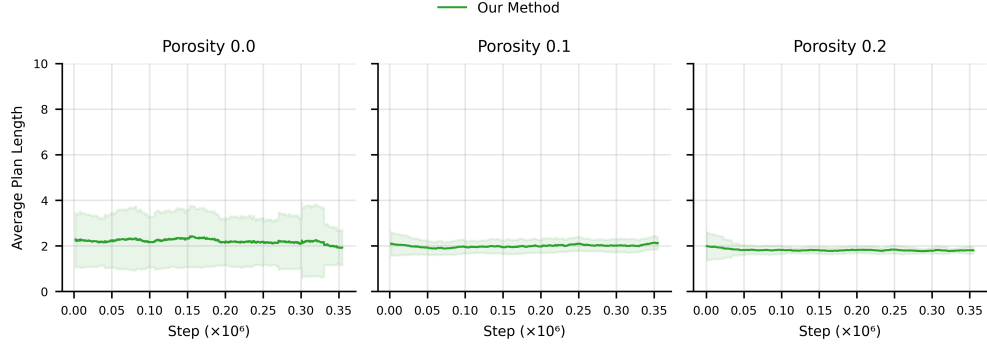


Figure 14: Length of plan before replanning across porosities. Stability is observed overall, with higher inter-seed variation in low-porosity settings.

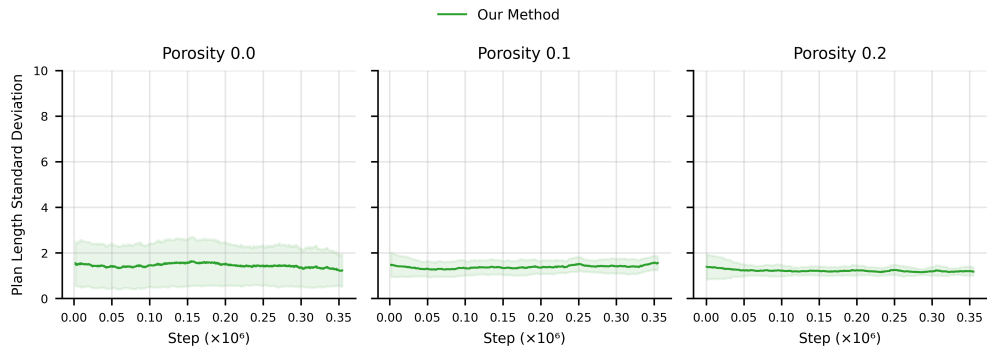


Figure 15: Intra-episode standard deviation of plan length before replanning. Values remain low across porosities, suggesting consistent behavior within each run.